

Analytical E1 strength functions of two-neutron halo nuclei: ^{11}Li and ^{14}Be

C. Forssén^{a,*}, V. D. Efros^b and M. V. Zhukov^a

^a*Department of Physics, Chalmers University of Technology and Göteborg University, S-412 96 Göteborg, Sweden*

^b*The Kurchatov Institute, 123182 Moscow, Russia*

Abstract

An analytical model, recently developed to study the electromagnetic dissociation (EMD) energy spectra of two-neutron halo nuclei, is applied to ^{11}Li and ^{14}Be . We find that a reliable set of experimental data on EMD could help to resolve the problem concerning the structure of the ^{11}Li ground state. For ^{14}Be we find a mutual inconsistency between the existing experimental data on the binding energy, radius and EMD energy spectrum. We also conclude that the structure of ^{14}Be is essentially more complicated than the structure of other Borromean two-neutron halo nuclei.

Key words: Borromean halo nuclei, three-body model, electromagnetic dissociation, strength function, continuum excitations

PACS: 25.70.De; 21.60.Gx; 24.10.-i; 27.20.+n

1 Introduction

The reaction of Coulomb excitation in collisions with heavy targets is an important tool to study the structure of unstable nuclei. For nuclei having only one bound state the excitation means breakup and the process is called electromagnetic dissociation (EMD). In the present paper E1 EMD of two-neutron halo nuclei is considered. Microscopic calculations of the process at the three-cluster level were performed for ^6He [1,2], ^{11}Li [2,3], and ^{14}Be [4,5]. Such calculations are hindered by incomplete knowledge of the cluster dynamics. Quantum Monte Carlo A-nucleon calculations [6] are hindered by

* Corresponding author.

Email address: c.forssen@fy.chalmers.se (C. Forssén).

the complexity of the A -body problem. Therefore it seems to be of interest to describe the process semi-phenomenologically aiming both to understand its main features and to guide experimental studies. Such an approach was developed in our recent paper [7]. Three-cluster bound-state wave functions (WFs) of two-neutron halo nuclei were constructed which behave correctly at large intercluster distances, reproduce the nuclear sizes, and incorporate the main features of the underlying three-body structure. No-interaction three-body WFs were used to describe the breakup final states. The model allows an analytic calculation of the strength functions and can serve as a tool to predict the Coulomb disintegration spectra of a variety of two-neutron halo nuclei. It may be used when precise knowledge concerning the structure of a system under study is lacking. As a test case the relatively well-studied nucleus ${}^6\text{He}$ was considered in [7]. We found that the large-distance asymptotics of the ground-state WF determines the shape and the position of the maximum of the strength function, while the size of the ground state governs the asymptotic constant and thus the magnitude of the strength function. As to the final-state interaction (FSI) effects, one can note that the total E1 strength will not change when replacing a complete set of true final states with a complete set of no-interaction final states. Therefore the inclusion of FSI will result only in a redistribution of the strength leading to a somewhat higher strength at low energies. But even without including FSI a very good agreement concerning the shape and peak position of the E1 strength function and a reasonable agreement concerning its magnitude was found in the ${}^6\text{He}$ case [7].

In the present paper we apply the model to study the Borromean halo nuclei ${}^{11}\text{Li}$ and ${}^{14}\text{Be}$. For both nuclei there are large ambiguities concerning the ground-state structure. Furthermore, there are large uncertainties in the experimental data regarding EMD reactions and, for ${}^{14}\text{Be}$, also concerning basic ground-state quantities such as binding energy and size. Therefore we believe that an analytical model with large freedom in trying different assumptions can be very useful.

In Sec. 2 the model is outlined, more details can be found in Ref. [7]. In Sec. 3 the results of our analysis of the ${}^{11}\text{Li}$ and ${}^{14}\text{Be}$ EMD data are presented. Sec. 4 contains the conclusions.

2 Analytical E1 strength functions of two-neutron halo nuclei

We consider the electromagnetic excitation of a system with only one bound state and consequently with all possible final states belonging to the continuum. In the framework of first-order perturbation theory the energy spectrum

for E1 Coulomb excitation can be written as

$$\frac{d\sigma(\text{E1})}{dE} = \frac{N_{\text{E1}}(E^*)}{\hbar c} \frac{16\pi^3}{9} \frac{dB(\text{E1})}{dE}. \quad (1)$$

Here E^* is the excitation energy, $E^* = E_0 + E$, where E_0 is the binding energy, and E is the continuum energy, $N_{\text{E1}}(E^*)$ is the spectrum of virtual photons [8,9] and $dB(\text{E1})/dE$ is the dipole strength function

$$\frac{dB(\text{E1})}{dE} = \frac{1}{2J_i + 1} \sum_{M_i} \sum_{\mu=-1,0,1} \int d\tau_f |\langle f | \mathcal{M}(\text{E1}, \mu) | i; J_i M_i \rangle|^2 \delta(E_f - E), \quad (2)$$

where $d\tau_f$ is the phase-space element for final states, $\mathcal{M}(\text{E1})$ is the dipole transition operator, $|i\rangle$ is the initial state, and $|f\rangle$ are the final states in the center-of-mass (CM) system. The notation $\int d\tau_f$ in Eq. (2) implies summation over discrete quantum numbers in addition to integration. We will study halo nuclei which are known to exhibit a large degree of clusterization. Since we are interested in low-energy excitations, involving mainly relative motion between the clusters, we will use the corresponding N -cluster E1 operator

$$\vec{\mathcal{M}}(\text{E1}) = \sqrt{\frac{3}{4\pi}} \sum_{i=1}^N e Z_i (\vec{r}_i - \vec{R}_{\text{cm}}), \quad (3)$$

where \vec{r}_i are the cluster positions, and \vec{R}_{cm} is the position of the CM of the system.

We adopt the three-body model to describe two-neutron halo nuclei. The cluster part of the bound-state WF, in the CM system, is written as an expansion over hyperspherical harmonics (HH), see e.g. [10],

$$\Psi(\vec{x}, \vec{y}) = \rho^{-5/2} \sum_{KLSl_x l_y} \chi_{KLS}^{l_x l_y}(\rho) \left[\Gamma_{KL}^{l_x l_y}(\Omega_5) \otimes \theta_S \right]_{JM}. \quad (4)$$

Here $\{\vec{x}, \vec{y}\}$ is the set of normalized Jacobi vectors where \vec{x} corresponds to the vector joining the two valence neutrons, and $\{\rho, \Omega_5\}$ are the hyperspherical coordinates in the $\{\vec{x}, \vec{y}\}$ space. The functions $\Gamma_{KL}^{l_x l_y}$ are HH, and θ_{SMS} ($S = 0, 1$) are the spin functions of the two valence neutrons. Since the HH expansion converges rapidly we retain only one, or a few, terms. Furthermore, since the hyperradial functions, $\chi_{KLS}^{l_x l_y}(\rho)$, should behave rather similarly at large ρ , which is the region of interest, we use the same hyperradial function for all terms retained in the expansion. These approximations lead to the following normalized WF for initial bound states having $J^\pi = 0^+$

$$\begin{aligned} \Psi(\vec{x}, \vec{y}) = & \frac{\chi^{(N)}(\rho)}{\rho^{5/2}} \left\{ \left[a_{00} \Gamma_{000}^{00}(\Omega_5) + a_{20} \Gamma_{200}^{00}(\Omega_5) \right. \right. \\ & \left. \left. + a_{40} \Gamma_{400}^{00}(\Omega_5) \right] \theta_{00} + a_{21} \left[\Gamma_{21}^{11}(\Omega_5) \otimes \theta_1 \right]_{J=0} \right\}. \end{aligned} \quad (5)$$

The coefficients a_{00} , a_{20} , a_{21} and a_{40} entering here are the amplitudes of various HH, $a_{00}^2 + a_{20}^2 + a_{21}^2 + a_{40}^2 = 1$. (In addition to the WF components used in [7], the $K = 4$ contribution is introduced here and in Eq. (9) below.) We consider hyperradial functions of the following two forms. The first is a simple normalized exponential

$$\chi^{(1)}(\rho) \equiv \sqrt{2\kappa_0} \exp(-\kappa_0\rho), \quad (6)$$

where the single free parameter κ_0 is fitted to the binding energy via $E_0 = (\hbar\kappa_0)^2/(2m)$, and m is the nucleon mass. This function reproduces the true asymptotic behaviour of Borromean three-body systems with two neutrons as constituents, see e.g. [11]. However, the three-body size $\langle \rho^2 \rangle$, and consequently the total size of the system, is underestimated with such a model. Therefore, we introduce a second hyperradial model function having two free parameters

$$\begin{aligned} \chi^{(2)}(\rho) &\equiv c [\exp(-\kappa_0\rho) - \exp(-\kappa_1\rho)], \\ \text{where } c &= \sqrt{\frac{2\kappa_0\kappa_1(\kappa_0 + \kappa_1)}{(\kappa_0 - \kappa_1)^2}}. \end{aligned} \quad (7)$$

The parameters κ_0 and κ_1 are fixed using experimental values of binding energy and rms radius, see [7]. The condition that $\kappa_1 > \kappa_0$ ensures that the second term decays faster than the first, and thus the correct large- ρ asymptotics is preserved.

We use a complete set of no-interaction final states that include just coordinate-space HH

$$\frac{J_{K+2}(\kappa\rho)}{(\kappa\rho)^2} \left[\Gamma_{KL}^{l_x l_y}(\Omega_5) \otimes \theta_S \right]_{JM}. \quad (8)$$

Alike the plane waves, these states are solutions to the free-space six-dimensional Schrödinger equation. The continuum energy is related to κ via $E = (\hbar\kappa)^2/(2m)$.

Using these model WFs an analytical calculation of the transition matrix elements (MEs) entering Eq. (2) is possible. When the model WF of Eqs. (5, 7) is adopted for the bound state, one obtains the following final expression for the E1 strength function:

$$\begin{aligned} \frac{dB(E1)}{dE} &= c^2 D E^3 \sum_{i,j=0}^1 \frac{(-1)^{i+j}}{[(E_i + E)(E_j + E)]^{11/4}} \\ &\times [\alpha_1 F_1(y_i) F_1(y_j) + \alpha_2 F_2(y_i) F_2(y_j) + \alpha_3 F_3(y_i) F_3(y_j)], \end{aligned} \quad (9)$$

Here $E_{0,1} = (\hbar\kappa_{0,1})^2/(2m)$, where κ_0 , κ_1 and c are defined in Eq. (7). The constant D is

$$D = \frac{3}{2} \left(\frac{\hbar^2}{2m} \right)^{3/2} \frac{(Z_c e)^2}{(A-2)A},$$

and the constants α_1 , α_2 and α_3 are

$$\begin{aligned}\alpha_1 &= \frac{1}{4} \left(\frac{315}{2^{10}} \right)^2 \left(4a_{00}^2 + a_{20}^2 + a_{21}^2 + 4a_{00}a_{20} \right), \\ \alpha_2 &= \left(\frac{9009\sqrt{3}}{2^{17}} \right)^2 \left(a_{20}^2 + a_{21}^2 + \frac{4}{9}a_{40}^2 + \frac{4}{3}a_{20}a_{40} \right), \\ \alpha_3 &= \frac{3}{2} \left(\frac{36465}{2^{20}} \right)^2 a_{40}^2.\end{aligned}$$

The coefficients a_{00} , a_{20} , a_{21} and a_{40} are defined in Eq. (5). The quantities $y_{0,1}$ are defined as $y_i = E/(E + E_i)$, and, finally,

$$\begin{aligned}F_1(y) &= F\left(\frac{11}{4}, \frac{3}{4}, 4, y\right), & F_2(y) &= yF\left(\frac{15}{4}, \frac{7}{4}, 6, y\right), \\ F_3(y) &= y^2F\left(\frac{19}{4}, \frac{11}{4}, 8, y\right),\end{aligned}$$

where $F(\alpha, \beta, \gamma, z)$ is the standard hypergeometrical function. The corresponding three terms in Eq. (9) represent contributions from final states with $K = 1$, $K = 3$ and $K = 5$ respectively. When the hyperradial function (6) is used the result is obviously obtained from Eq. (9) by retaining only the term with $i = j = 0$ and replacing c^2 with $2\kappa_0$.

3 Results

3.1 ^{11}Li

Despite the great number of experimental and theoretical studies that have been performed, the ^{11}Li nucleus still remains a puzzle. The role of possible s -wave intruder states [12–16] is of much theoretical interest. The experimental evidence for virtual s -states in the binary subsystem ^{10}Li is diverse and sometimes conflicting [17–24]. Three-body microscopic calculations of ^{11}Li are uncertain due to this fact, in particular. Note that whereas the most recent experiments establish that the ground state of ^{10}Li is a $s_{1/2}$ state [24], this itself does not mean that the $(s_{1/2})^2$ configuration is a predominant one in ^{11}Li . The weights of the $(s_{1/2})^2$ and $(p_{1/2})^2$ configurations depend on the relative strength of s - and p -wave potentials determining the gap between the $s_{1/2}$ and $p_{1/2}$ states in ^{10}Li . The shape of the ^{10}Li momentum distribution, measured in a ^{11}Li fragmentation reaction [25], supports a $(1s_{1/2})^2$ contribution of $(45 \pm 10)\%$ in the ^{11}Li ground-state WF. Further evidence for the mixing of different parity states is clearly seen in the asymmetric angular correlations [25].

Clearly, the present–time understanding of the structure of ^{11}Li is substantially poorer than that in the ^6He case, in which case more definite information on the interaction between the valence neutrons and the core is available. This makes ^{11}Li an interesting nucleus to study with our analytical model. In this way we will be able to test different assumptions on the ground–state structure. In the present work we have used four different ground–state WFs of ^{11}Li , which are summarized in Table 1. Here we restricted ourselves to HH with the lowest possible K values, $K = 0$ and $K = 2$. These configurations correspond, respectively, to the $(s_{1/2})^2$ and $(p_{1/2})^2$ configurations of the core–centered shell model for valence nucleons.

To explain the latter fact we need to consider a relationship between HH and the configurations of the core–centered shell model. One can pass from the Jacobi vectors $\{\vec{x}, \vec{y}\}$ defined in connection with Eq. (4) to another pair $\{\vec{x}_1, \vec{y}_1\}$ of Jacobi vectors, such that \vec{x}_1 is proportional to the distance between one of the valence nucleons and the core, and \vec{y}_1 is proportional to the distance between the other valence nucleon and the CM of the pair consisting of the former valence nucleon and the core. The distance from the CM of this pair to the core is A_c^{-1} times smaller than that to the valence nucleon belonging to the pair. In the framework of the approximation where one neglects the former distance as compared to the latter one, i.e. locates the CM of the pair on the core, the Jacobi orbital momenta associated with the vectors $\{\vec{x}_1\}$ and $\{\vec{y}_1\}$ coincide with orbital momenta of the two valence nucleons in the core–centered shell model. In order to find HH to be retained in the model WF we proceed as follows. Let $\Gamma_{KLM}^{l_x l_y}(\vec{x}, \vec{y})$ denote the HH entering Eq. (4). In addition, we define the HH $\Gamma_{KLM}^{l_{x_1} l_{y_1}}(\vec{x}_1, \vec{y}_1)$ where l_{x_1} and l_{y_1} are Jacobi orbital momenta associated with \vec{x}_1 and \vec{y}_1 . We consider first the expansion over the latter HH and we retain the terms in this expansion for which the orbital momenta L , l_{x_1} , and l_{y_1} are the same as for predominant configurations in the core–centered shell model. Note, however, that the corresponding HH do not coincide with the lowest shell–model configurations but also include higher shell–model states with radial excitations. The final formula (5) with the coefficients listed in Table 1 is obtained expressing the retained HH $\Gamma_{KLM}^{l_{x_1} l_{y_1}}(\vec{x}_1, \vec{y}_1)$ as linear combinations of the HH $\Gamma_{KLM}^{l_x l_y}(\vec{x}, \vec{y})$. The quantum numbers K and L are conserved at this transformation of HH.

The first two of our WFs are 100% $K = 0$ states. In the case of $K = 0$ states the orbital momenta of relative motion in each pair of the three particles are zeros. Thus the $K = 0$ state corresponds to the $(s_{1/2})^2$ configuration of the core–centered shell model. The wave function $\Psi_1(^{11}\text{Li})$ contains the one–parameter hyperradial function (6) while $\Psi_2(^{11}\text{Li})$ contains the two–parameter function (7).

The two other WFs, $\Psi_3(^{11}\text{Li})$ and $\Psi_4(^{11}\text{Li})$, include HH with $K = 0$ and $K = 2$. They correspond to 50% mixtures of $(s_{1/2})^2$ and $(p_{1/2})^2$ configurations.

To obtain the $K = 2$ HH and their weights listed in Table 1 we expand the $(p_{1/2})^2$, $J = 0$ neutron shell-model state over such states in LS coupling. In the framework of our infinite core-mass approximation the latter states correspond to HH, $\Gamma_{KLM}^{l_1 l_2}$, with $K = 2$ and $l_1 = l_2 = 1$, defined with respect to the above mentioned Jacobi vectors $\{\vec{x}_1, \vec{y}_1\}$. Two such HH arise, one with $L = 1$, and the other with $L = 0$. Finally, when the above mentioned rotation to the $\{\vec{x}, \vec{y}\}$ system is performed the first HH (with $L = 1$) transforms into a single HH with $K = 2$, $L = l_x = l_y = 1$ and the second one (with $L = 0$) transforms into a single HH with $K = 2$, $L = l_x = l_y = 0$.

The WF $\Psi_4(^{11}\text{Li})$ differs from $\Psi_3(^{11}\text{Li})$ only in that the relative signs of the amplitudes pertaining to the $(p_{1/2})^2$ configuration and the $(s_{1/2})^2$ configuration are different.

The results of our calculation are presented in Fig. 1 along with available experimental data. The E1 strength functions are plotted in the figure. In Fig. 1(a) the results are presented in arbitrary units and in Fig. 1(b) they are plotted in absolute scale. There exist three published sets of experimental data on EMD which show large ambiguities. The experiments were performed at different energies, Zinser *et al.* [26] used a high energy beam (280 MeV/A) while Sackett *et al.* [27] and Shimoura *et al.* [28] had much lower energy, 28 and 43 MeV/A, respectively. The validity of extracting the E1 strength function from the low-energy experiments [27,28] is discussed in [27]. Sackett *et al.* report their data only up to $E = 1.45$ MeV above particle-decay threshold, and Shimoura *et al.* list their strength function only in arbitrary units due to the lack of a forward-angle detector. In the Zinser *et al.* experiment, the strength function was decomposed into two Gaussian components. The two-peak structure observed by Zinser *et al.* was not seen in the other two experiments. It is clear that the data sets are contradictory. The shapes are different, and the peak amplitude is much higher in the Sackett *et al.* data than in the Zinser *et al.* data. However, in all data sets the position of the maximum is approximately the same.

Our results may be commented as follows. All our ground-state WFs give the peak position at about $0.5 - 0.7$ MeV which is very close to all experimental findings. This value is expected. Indeed, for not too high energy the predominant contribution to the strength function comes from large distances, and in our model it is provided by the first, longer range exponential in Eq. (7), see also [7]. Because of this the strength function is mainly a function of E/E_0 . Moreover, in the peak region the dominating final state has $K = 1$ which corresponds to the contribution of the single term with F_1 in Eq. (9). Due to these facts the positions of the peak are close to each other for all our ground-state WFs and proved to be about $2E_0$, see also [29]. However, terms with larger K in (9) change the behaviour at higher energies. There is no possibility to explain the two-peak structure of Zinser *et al.* in our model. The one-parameter

WF, $\Psi_1(^{11}\text{Li})$, leads to a very low strength which is expected since it underestimates the size of the system, see Table 1. The results obtained with our three other model ground-state WFs of ^{11}Li are to be compared with experiment if the absolute values of the strength function are considered.

We see that the $\Psi_2(^{11}\text{Li})$ WF, which corresponds to s -motion of the valence neutrons with respect to the core and also to relative s -motion between them (or a $(s_{1/2})^2$ configuration in core-centered, shell-model coordinates), compares rather well with the Sackett *et al.* data. However, for energies $E > 0.5$ MeV the error bars in [27] are large. On the contrary, the $\Psi_3(^{11}\text{Li})$ WF, where we have equal weights of $(s_{1/2})^2$ and $(p_{1/2})^2$ configurations in ^{11}Li , leads to an excellent agreement with the shape of the Shimoura *et al.* data and a relatively good agreement with the absolute values of the Zinser *et al.* data. Finally, the $\Psi_4(^{11}\text{Li})$ WF leads to results which are significantly different from those obtained with $\Psi_3(^{11}\text{Li})$. This may be related to the fact that the corresponding difference in the relative sign of the $(s_{1/2})^2$ and $(p_{1/2})^2$ components of the WF leads to a change of the internal geometry of the system, and the r_c value in particular, as it is seen from Table 1. Thus there exists a sensitivity to the relative sign of the two components in the WF and not only to their weights. In conclusion we state that this kind of analysis, when applied to a reliable set of experimental EMD data, would give valuable information concerning the relative role of the $(s_{1/2})^2$ and $(p_{1/2})^2$ configurations in the ^{11}Li ground state.

3.2 ^{14}Be

The existing experimental data on ^{14}Be are scarce. Even such a fundamental quantity as the binding energy is characterized by large uncertainties. Combining the two published measurements gives the tabulated two-neutron separation energy of 1.34 ± 0.11 MeV [30,31]. The most recent value of the rms radius is 3.10 ± 0.15 fm [32]. Experimental and theoretical efforts are presently focused on understanding the ground-state structure. Assuming ^{12}Be to be a nucleus where the neutron p -shell is closed one gets $0d_{5/2}$ as the next orbital for the valence neutrons. Several experiments have indeed confirmed a state around 2 MeV in ^{13}Be which is assigned having spin-parity $I^\pi = 5/2^+$ [33–36]. However, in order to reproduce the large size and narrow momentum distributions, a large s -wave component is needed in the ground state of ^{14}Be [4,5]. The s -wave potential fitted in [4,5] to reproduce the ^{14}Be binding energy, with the known position of the $d_{5/2}$ state, leads to an s -wave bound state in ^{13}Be which is clearly not observed. This problem may be connected with the fact that the ^{12}Be nucleus has no closed neutron p -shell (see [37,38]) and this effect has not been taken into account in [5]. Recent experiments still indicate the presence of a low-lying virtual s -wave state in ^{13}Be [36]. Furthermore,

studies of the isobaric analog state of ^{14}Be give an s –wave spectroscopic factor of $45 \pm 20\%$ in the ^{14}Be ground state [39] which is supported by conclusions made in other experiments [32,40]. The $K = 0$ component of our model WF provides s –motion between all the particles, and we used the $K = 4$ component to include some d –motion. However, since the $K = 4$ component leads to a very broad distribution of strength the shape will mainly be determined by the $K = 0$ component.

The EMD energy spectrum for ^{14}Be has recently been measured by Labiche *et al.* [40]. This experiment was performed at 35 MeV/A. In their analysis the energy spectrum was modeled using the Breit–Wigner shape with parameters $E_{\text{BW}} = 1.8 \pm 0.1$ MeV and $\Gamma_{\text{BW}} = 0.8 \pm 0.4$ MeV, see Fig. 2 in [40]. We prefer to compare theory and experiment using strength functions which facilitates comparison with EMD cross sections for other nuclei and at other beam energies as well. We therefore extracted the dipole strength function from the EMD spectrum of Ref. [40] dividing out the virtual photon spectrum entering Eq. (1). This results in a very narrow distribution peaked just below 2 MeV as can be seen from Fig. 2. Note that the shape of this strength function is very different from those of strength functions of other Borromean halo nuclei. It should also be mentioned that in the experiment [40] only ^{12}Be and neutrons were detected. Therefore, we should consider the strength function up to the ^{12}Be threshold at 3.2 MeV because above this energy other reaction channels are open.

In a first step of the analysis we use the position of the peak to check the binding energy. If the ground–state WF has an appreciable $K = 0$ weight then, as mentioned above, the peak should be positioned at approximately $2E_0$. As can be seen from Fig 2(a) the experimental spectrum would correspond to a binding energy of $E_0 \approx 0.9$ MeV, considerably lower than the tabulated value of 1.34 MeV. In fact, we have one more indication that the tabulated binding energy is too large. Namely, the binding energy seems to be incompatible with the radius of ^{14}Be . In Table 2 we compare the hyperradii

$$\rho_{\text{rms}} = \left\langle \sum_{i=1}^3 A_i (\vec{r}_i - \vec{R}_{\text{cm}})^2 \right\rangle^{1/2}$$

of ^6He , ^{11}Li and ^{14}Be which represent the three–body sizes of the systems. They are calculated from the rms radii of these nuclei and their three–body constituents. For halo nuclei the hyperradii are mainly determined by the asymptotic behavior of the WFs. Therefore their values should exhibit a correlation with binding energies. Due to this reason one would expect from the systematics of ^6He and ^{11}Li that either the binding energy of ^{14}Be should be smaller at given size or the size should be smaller at given energy.

Examples of $K = 0$ ground–state WFs that we have used are summarized

in Table 3. We were unable to reproduce both binding energy and size with the two-parameter hyperradial function (7). In the limit $\kappa_1 \rightarrow \kappa_0$ we get $R_{\text{rms}} = 3.0$ fm. The asymptotic behaviour of the WF changes in this limit. In order to reproduce both binding energy and size we have used one more model hyperradial function

$$\chi^{(3)}(\rho) \equiv N_0 \left(\frac{\rho}{\rho + \rho_0} \right)^{5/2} \exp(-\kappa_0 \rho) \quad (10)$$

which behaves correctly both at large and small ρ . The strength functions, obtained with the one-parameter function $\Psi_1(^{14}\text{Be})$ and with the two-parameter function of Eq. (10) $\Psi_3(^{14}\text{Be})$, are compared in Fig. 2(b). Note that the transition ME must be calculated numerically when (10) is used. We see that unlike the ^6He [7] and ^{11}Li cases the low-energy part of the strength function, and thus the peak position, changes substantially when going from the one- to the two-parameter WF. This happens due to the fact that, at the binding energy and size of ^{14}Be used for fitting our bound-state WF, the non-asymptotic part of the hyperradial function contributes noticeably to the results.

We also tried to vary the binding energy, the radius and the admixture of different components in the ground-state WF. However in all the cases we were unable to reproduce the narrow width and large amplitude of the experimental spectrum. A dominant $K = 4$ component in the ground-state WF leads to a very broad distribution of E1 strength with a small maximum at high energy (about $5E_0$). When initial and final state WFs are obtained from model interparticle potentials, such as the D4 potential of Ref. [5], it is also not possible to reproduce the shape of the spectrum. Thus inclusion of FSI does not solve the problem. (Note that while the D4 WF reproduces the binding energy and the size of ^{14}Be the corresponding potential leads to an unphysical s -wave bound state in ^{13}Be .)

In Table 4 we compare the integrated strength extracted from the experimental data [40] with the strengths obtained with our $\Psi_3(^{14}\text{Be})$ WF and with the D4 WF of Ref. [5]. When the integration is performed up to the ^{12}Be threshold the theoretical strengths prove to be substantially lower than the experimental one. Furthermore, an estimate of the strength integrated up to infinity can be made using the experimental radius, $R_{\text{rms}} = 3.10 \pm 0.15$ fm [32], together with the E1 non-energy-weighted cluster sum rule

$$\int_0^\infty \frac{dB(\text{E1})}{dE} dE = \frac{3}{4\pi} Z_c^2 e^2 \langle r_c^2 \rangle. \quad (11)$$

A simple relation between R_{rms} and the distance r_c between the CM and the core in a three-body picture is obtained by assuming $\langle x^2 \rangle = \langle y^2 \rangle = \langle \rho^2 \rangle / 2$

(see Appendix A.1 of Ref. [7]). This gives

$$\langle r_c^2 \rangle = \frac{R_{\text{rms}}^2(A)}{A_c} - \frac{R_{\text{rms}}^2(A_c)}{A}.$$

It is clear that the integrated strength obtained from the EMD experiment [40] is too large as compared with the estimates in the table. To fit the experimental strength one needs a larger size of ^{14}Be while the correlation with binding energy requires a smaller size. Thus we encounter one more inconsistency.

In conclusion, we state that there are mutual disagreements between existing experimental data on the binding energy [30,31], the radius [32], and the EMD energy spectrum [40] of ^{14}Be . In our three-body model we are unable to reproduce these data all at once. This result is in line with previous microscopic studies of ^{14}Be [4,5,41] and in contrast with our results for other halo nuclei. At the same time we can confirm that a large s -wave component in the ^{14}Be ground state is required to obtain an accumulation of E1 strength at low energies.

4 Discussion

In Ref. [7] our analytical model was tested on the relatively well-known ^6He nucleus. In the present paper we have studied ^{11}Li and ^{14}Be for which both experimental data and theoretical understanding are much poorer. Concerning ^{11}Li we conclude that data on E1 strength functions, analyzed in the framework of our model, can help to resolve the issue on the relative content of $(s_{1/2})^2$ and $(p_{1/2})^2$ components in the ground state of ^{11}Li . However, the existing sets of EMD data are not consistent with each other. As our calculations show, the E1 strength function of Sackett *et al.* [27] seems to favor a configuration with a dominant $(s_{1/2})^2$ component while the data of Zinser *et al.* [26] and Shimoura *et al.* [28] are more in agreement with a mixture of $(s_{1/2})^2$ and $(p_{1/2})^2$ components with equal weights.

Regarding ^{14}Be we have analyzed the available experimental data on EMD and found disagreements between these data, the measured size, and the binding energy. In the framework of our model it also proved to be impossible to reproduce the narrow width of the strength function. This is in contrast with the results for other two-neutron halo nuclei. A theoretical study of ^{14}Be based on model intercluster potentials led to a similar disagreement [5]. This disagreement is thus not due to the neglection of FSI. The considerable weight of the $(p_{1/2})^2$ component in ^{14}Be WF, suggested in [41], will also not help to reduce the width in our model. There is a possibility that the structure of ^{14}Be is more complicated than for other Borromean, two-neutron halo nuclei. Perhaps ^{14}Be

has more in common with ^8He than with ^6He in which case calculations should be done in the framework of a five–body model or should include excited–core configurations. More complete experimental data on neutron–removal cross sections could help to clarify whether ^{14}Be has a three–cluster or five–cluster structure. The five–body analysis of the experimental data on interaction cross sections, similar to that performed for ^8He [42], would give a slightly smaller size of ^{14}Be than the size obtained in the framework of a three–body picture [32]. However, in a five–body model the E1 strength would probably have an even broader distribution still not allowing the reproduction of the experimental EMD data of Labiche *et al.* [40]. Furthermore, methods to measure masses of short–lived isotopes have improved significantly since the experiments [30,31] were performed, and new experimental results on the ^{14}Be mass would be very important.

Acknowledgements

This work is supported by NFR, Sweden, contract F5102–1484/2001 (C.F., M.V.Z.) and RFBR, Russia, grant 00–15–96590 (V.D.E.). V.D.E. also acknowledges support from the Royal Swedish Academy of Sciences contract for cooperation between Sweden and former Soviet Union.

References

- [1] B. V. Danilin, I. J. Thompson, J. S. Vaagen, and M. V. Zhukov, Nucl. Phys. A **632**, 383 (1998).
- [2] A. Cobis, D. V. Fedorov, and A. S. Jensen, Phys. Rev. C **58**, 1403 (1998).
- [3] I. J. Thompson, B. V. Danilin, V. D. Efros, M. V. Zhukov, and J. S. Vaagen, J. Phys. G **24**, 1505 (1998).
- [4] P. Descouvemont, Phys. Rev. C **52**, 704 (1995).
- [5] I. J. Thompson and M. V. Zhukov, Phys. Rev. C **53**, 708 (1996).
- [6] V. R. Pandharipande, Nucl. Phys. A **654**, 157c (1999).
- [7] C. Forssén, V. D. Efros, and M. V. Zhukov, Nucl. Phys. A **697**, 639 (2002).
- [8] A. Winther and K. Alder, Nucl. Phys. A **319**, 518 (1979).
- [9] C. A. Bertulani and G. Baur, Nucl. Phys. A **442**, 739 (1985).
- [10] M. V. Zhukov et al., Phys. Rep. **231**, 151 (1993).
- [11] S. P. Merkuriev, Sov. J. Nucl. Phys. **19**, 222 (1974).

- [12] L. Johannsen, A. S. Jensen, and P. G. Hansen, *Phys. Lett. B* **244**, 357 (1990).
- [13] I. J. Thompson and M. V. Zhukov, *Phys. Rev. C* **49**, 1904 (1994).
- [14] K. Ueta, H. Miyake, and G. W. Bund, *Phys. Rev. C* **59**, 1806 (1999).
- [15] T. Suzuki, H. Sagawa, and P. F. Bortignon, *Nucl. Phys. A* **662**, 282 (2000).
- [16] E. Garrido, D. V. Fedorov, and A. S. Jensen, *Nucl. Phys. A* **700**, 117 (2002).
- [17] K. H. Wilcox et al., *Phys. Lett. B* **59**, 142 (1975).
- [18] A. I. Amelin et al., *Sov. J. Nucl. Phys.* **52**, 782 (1990).
- [19] B. M. Young et al., *Phys. Rev. C* **49**, 279 (1994).
- [20] M. Zinser et al., *Phys. Rev. Lett.* **75**, 1719 (1995).
- [21] H. G. Bohlen et al., *Nucl. Phys. A* **616**, 254c (1997).
- [22] M. Thoennessen et al., *Phys. Rev. C* **59**, 111 (1999).
- [23] J. A. Caggiano et al., *Phys. Rev. C* **60**, 064322 (1999).
- [24] M. Chartier et al., *Phys. Lett. B* **510**, 24 (2001).
- [25] H. Simon et al., *Phys. Rev. Lett.* **83**, 496 (1999).
- [26] M. Zinser et al., *Nucl. Phys. A* **619**, 151 (1997).
- [27] D. Sackett et al., *Phys. Rev. C* **48**, 118 (1993).
- [28] S. Shimoura et al., *Phys. Lett. B* **348**, 29 (1995).
- [29] A. Pushkin, B. Jonson, and M. V. Zhukov, *J. Phys. G* **22**, 95 (1996).
- [30] R. Gilman et al., *Phys. Rev. C* **30**, 958 (1984).
- [31] J. M. Wouters, R. H. Kraus Jr., D. J. Vieira, G. W. Butler, and K. E. G. Löbner, *Z. Phys. A* **331**, 229 (1988).
- [32] T. Suzuki et al., *Nucl. Phys. A* **658**, 313 (1999).
- [33] A. N. Ostrowski et al., *Z. Phys. A* **343**, 489 (1992).
- [34] A. A. Korsheninnikov et al., *Phys. Lett. B* **343**, 53 (1995).
- [35] A. V. Belozyorov et al., *Nucl. Phys. A* **636**, 419 (1998).
- [36] M. Thoennessen, S. Yokoyama, and P. G. Hansen, *Phys. Rev. C* **63**, 014308(3) (2000).
- [37] A. Navin et al., *Phys. Rev. Lett.* **85**, 266 (2000).
- [38] H. Iwasaki et al., *Phys. Lett. B* **481**, 7 (2000).
- [39] S. Takeuchi, S. Shimoura et al., *Phys. Lett. B* **515**, 255 (2001).

- [40] M. Labiche et al., Phys. Rev. Lett. **86**, 600 (2001).
- [41] M. Labiche, F. M. Marqués, O. Sorlin, and N. Vinh Mau, Phys. Rev. C **60**, 027303(3) (1999).
- [42] J. S. Al-Khalili and J. A. Tostevin, Phys. Rev. C **57**, 1846 (1998).

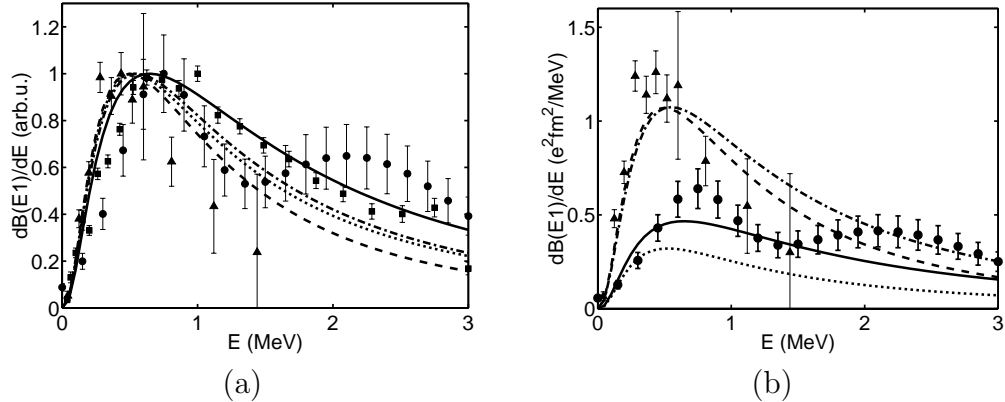


Fig. 1. A comparison of our strength function with experimental data for ^{11}Li (circles [26], triangles [27], squares [28]), both in arbitrary units (a) and in absolute scale (b). The model WFs are: dotted – $\Psi_1(^{11}\text{Li})$, dashed – $\Psi_2(^{11}\text{Li})$, solid – $\Psi_3(^{11}\text{Li})$, dash-dotted – $\Psi_4(^{11}\text{Li})$, see Table 1.

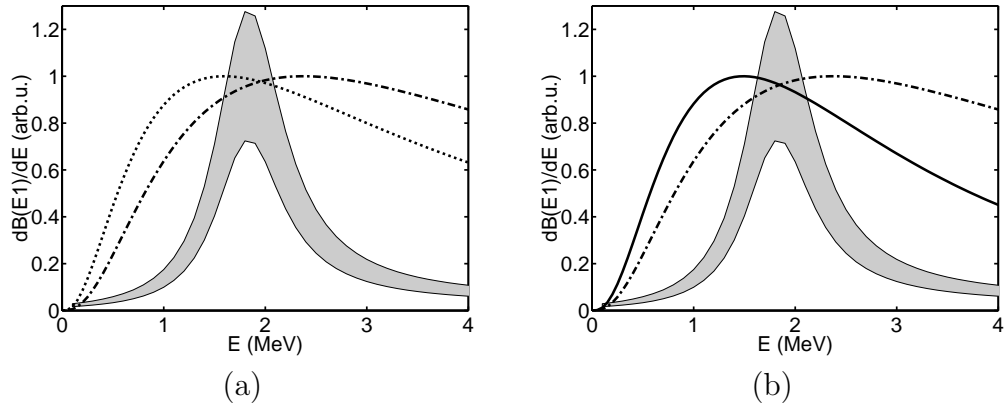


Fig. 2. The positions of the peak obtained with two different binding energies of ^{14}Be (a). The curves correspond to the one-parameter function (6) with $E_0 = 1.34$ MeV (dash-dotted) and $E_0 = 0.90$ MeV (dotted). In (b) it is shown how the distribution changes when trying to fit both binding energy and size. Here the solid curve corresponds to the two-parameter $\Psi_3(^{14}\text{Be})$ WF, Eq. (10), which reproduces both these quantities, while the dash-dotted curve is the same as in (a). In both figures a comparison is made with "experimental data" obtained by dividing out the spectrum of virtual photons from the energy spectrum of Ref. [40].

Table 1

The model WFs for ^{11}Li . To reproduce binding energy and rms radius we use $\kappa_0 = 0.1193 \text{ fm}^{-1}$ and $\kappa_1 = 0.3173 \text{ fm}^{-1}$. The quantity r_c is the distance between the core and the CM. The approximate amplitudes of $(s_{1/2})^2$ and $(p_{1/2})^2$ configurations of valence neutrons are shown in the last two columns.

WF	$\chi(\rho)$	a_{00}	a_{20}	a_{21}	R_{rms}	r_c	$a_{(s_{1/2})^2}$	$a_{(p_{1/2})^2}$
	Eq.				(fm)	(fm)		
$\Psi_1(^{11}\text{Li})$	(6)	1	0	0	2.76	0.60	1	0
$\Psi_2(^{11}\text{Li})$	(7)	1	0	0	3.55	0.95	1	0
$\Psi_3(^{11}\text{Li})$	(7)	$\sqrt{1/2}$	$-\sqrt{1/6}$	$\sqrt{1/3}$	3.55	0.80	$\sqrt{0.5}$	$\sqrt{0.5}$
$\Psi_4(^{11}\text{Li})$	(7)	$\sqrt{1/2}$	$\sqrt{1/6}$	$-\sqrt{1/3}$	3.55	1.08	$\sqrt{0.5}$	$-\sqrt{0.5}$

Table 2

Comparison of hyperradii and binding energies of three Borromean halo nuclei.

Nucleus	E_0 (MeV)	ρ_{rms} (fm)
^{11}Li	0.295	9.5
^6He	0.97	5.4
^{14}Be	1.34	7.4

Table 3

The model WFs for ^{14}Be . The binding energy of $E_0 = 1.34 \text{ MeV}$ corresponds to $\kappa_0 = 0.2543 \text{ fm}^{-1}$ while $E_0 = 0.90 \text{ MeV}$ corresponds to $\kappa_0 = 0.2084 \text{ fm}^{-1}$. The parameter ρ_0 entering the $\Psi_3(^{14}\text{Be})$ WF, Eq. (10), equals 5.42 fm. The quantity r_c is the distance between the core and the CM. Only the $K = 0$ term in the HH expansion has been retained.

WF	$\chi(\rho)$	E_0	R_{rms}	r_c
	Eq.	(MeV)	(fm)	(fm)
$\Psi_1(^{14}\text{Be})$	(6)	1.34	2.51	0.21
$\Psi_2(^{14}\text{Be})$	(6)	0.90	2.56	0.26
$\Psi_3(^{14}\text{Be})$	(10)	1.34	3.10	0.57

Table 4

Experimental and theoretical integrated E1 strengths. The first row represents strengths integrated up to 3.2 MeV (^{12}Be threshold). In the second row total strengths are shown. The total strength in the second column is calculated from the value $R_{\text{rms}} = 3.10 \pm 0.15$ fm [32] using the non-energy-weighted cluster sum rule. To this aim, the r_c value of 0.57 ± 0.07 fm was obtained from the above value of R_{rms} assuming a simple three-body structure.

	Extracted from [40]	Obtained from R_{rms} [32]	$\Psi_3(^{14}\text{Be})$	D4 [5]
$B_{E<3.2}(\text{E1}) (e^2\text{fm}^2)$	1.40 ± 0.40		0.70	0.96
$B(\text{E1}) (e^2\text{fm}^2)$		1.23 ± 0.33	1.23	1.56